

Single-photon double ionization: renormalized-natural-orbital theory *vs* multi-configuration Hartree-Fock

M. Brics, J. Rapp, and D. Bauer

Institut für Physik, Universität Rostock, 18051 Rostock, Germany

(Dated: December 14, 2024)

The N -particle wavefunction has too many dimensions for a direct time propagation of a many-body system according to the time-dependent Schrödinger equation (TDSE). On the other hand, time-dependent density functional theory (TDDFT) tells us that the single-particle density is, in principle, sufficient. However, a practicable equation of motion (EOM) for the accurate time evolution of the single-particle density is unknown. It is thus an obvious idea to propagate a quantity which is not as reduced as the single-particle density but less dimensional than the N -body wavefunction. Recently, we have introduced time-dependent renormalized natural orbital theory (TDRNOT). TDRNOT is based on the propagation of the eigenfunctions of the one-body reduced density matrix (1-RDM), the so-called natural orbitals. In this paper we demonstrate how TDRNOT is related to the multi-configuration time-dependent Hartree-Fock (MCTDHF) approach. We also compare the performance of MCTDHF and TDRNOT *vs* the TDSE for single-photon double ionization (SPDI) of a 1D helium model atom. SPDI is one of the effects where TDDFT does not work in practice, especially if one is interested in correlated photoelectron spectra, for which no explicit density functional is known.

PACS numbers: 32.80.Fb, 31.15.ee, 31.70.Hq, 02.70.-c

Keywords: single-photon double ionization; correlated photoelectron spectra; density matrices; time-dependent density functional theory; multi-configuration time-dependent Hartree-Fock

I. INTRODUCTION

Single-photon double ionization (SPDI) is a prime example for a highly correlated atomic process: one photon is absorbed by an $N > 1$ -electron system, followed by the emission of two electrons. As the laser-atom interaction term in the Hamiltonian involves only one-electron operators, the photon interacts only with one electron directly, whose energy can then be shared via Coulomb interaction with another electron. SPDI of helium has been studied for 50 years now [1] and is still of interest to date [2]. Thanks to the increasing availability of free electron laser (FEL) sources, time-resolved studies of correlated or collective processes following the absorption of an XUV photon are within reach now (see, e.g., [3]).

In this work, we employ SPDI as a demanding benchmark for the recently developed time-dependent renormalized natural orbital theory (TDRNOT) [4–8] and the widely known multi-configuration time-dependent Hartree-Fock (MCTDHF) [9–11]. We work out the connection between TDRNOT and MCTDHF and benchmark their performance with a 1D helium model atom, for which the time-dependent Schrödinger equation (TDSE) is still numerically exactly solvable.

The development of powerful time-dependent quantum many-body approaches beyond linear response is one of the great challenges in theoretical and computational physics. In fact, a full numerical solution of the time-dependent Schrödinger equation (TDSE) for strong-field problems in full dimensionality is impossible for more than two electrons [12]. Unfortunately, efficient methods such as time-dependent density functional theory (TDDFT) [13, 14] fail, in particular if strong correlations are involved [15, 16]. In TDDFT, also some of the observables of interest cannot be expressed explicitly in terms of the single-particle density [15, 17]. It is thus an obvious idea to propagate a quantity which is not as re-

duced as the single-particle density but less dimensional than the wavefunction. Prominent candidates for such quantities are reduced density matrices [18–22].

In recent years, we introduced a novel method that goes one step beyond TDDFT as far as the complexity of the propagated quantity is concerned. In TDRNOT [4–8], the basic quantities that are propagated are the eigenfunctions of the one-body reduced density matrix (1-RDM), normalized to their eigenvalues, the so-called renormalized natural orbitals (RNO). There are also other wavefunction-based approaches available in the literature which overcome the problems of TDDFT [23, 24]. The most frequently used are MCTDHF [9–11] and time-dependent configuration interaction (TDCI) [25–27].

The paper is organized as follows. The theoretical method and the connection between TDRNOT and MCTDHF is described in Sec. II. In Sec. III, we benchmark and compare the performance of TDRNOT and MCTDHF regarding SPDI. We conclude in Sec. IV.

Atomic units (a.u.) are used throughout unless noted otherwise.

II. THEORETICAL METHODS

In this Section, we relate the recently introduced TDRNOT to MCTDHF by deriving the equations of motion (EOM) for both. Further, the model system we use to compare the performances of MCTDHF and TDRNOT is introduced.

A. Equations of motion (EOM)

The time-evolution of the N -particle state $|\Phi(t)\rangle$ is described via the TDSE

$$i\frac{\partial}{\partial t}|\Phi(t)\rangle = \hat{H}(t)|\Phi(t)\rangle. \quad (1)$$

The EOM for the N -body density matrix (N-DM) of a pure state

$$\hat{\gamma}_N(t) = |\Phi(t)\rangle\langle\Phi(t)| \quad (2)$$

is obtained by taking the time derivative of (2) and using the TDSE (1).

With an N -particle Hamiltonian of the form

$$\hat{H}(t) = \sum_{i=1}^N \left(\hat{h}^{(i)}(t) - i\hat{\Gamma}_e^{(i)} \right) + \sum_{i < j}^N \hat{v}_{ee}^{(i,j)} \quad (3)$$

where $\hat{h}(t)$ is the hermitian part of the single-particle Hamiltonian consisting of kinetic energy, electron-nucleus interaction, and electron interaction with external fields, e.g., the laser field, $-i\hat{\Gamma}_e$ is an imaginary potential for absorbing outgoing electron flux, and $\hat{v}_{ee}^{(i,j)}$ is the electron-electron interaction potential where the upper indices indicate that the operator is acting on electrons i and j . The EOM for the N-DM reads

$$\begin{aligned} i\partial_t\gamma_N(t) = & \sum_{i=1}^N \left[\hat{h}^{(i)}(t), \hat{\gamma}_N(t) \right] + \sum_{i < j}^N \left[\hat{v}_{ee}^{(i,j)}, \hat{\gamma}_N(t) \right] \\ & - i \sum_{j=1}^N \left[\hat{\Gamma}_e^{(j)}, \hat{\gamma}_N(t) \right]_+. \end{aligned} \quad (4)$$

By applying partial traces of (4) one can derive EOMs for the n -RDMs

$$\hat{\gamma}_n(t) = \binom{N}{n} \text{Tr}_{n+1, \dots, N} \hat{\gamma}_N(t). \quad (5)$$

The EOM for 1-RDM reads

$$\begin{aligned} i\dot{\hat{\gamma}}_1(t) = & \left[\hat{h}(t), \hat{\gamma}_1(t) \right] + 2\text{Tr}_2 \left[\hat{v}_{ee}, \hat{\gamma}_2(t) \right] - i \left[\hat{\Gamma}_e, \hat{\gamma}_1(t) \right]_+ \\ & - 2i\text{Tr}_2 \left[\hat{\Gamma}_e^{(2)}, \hat{\gamma}_2(t) \right]_+, \end{aligned} \quad (6)$$

where $[\hat{a}, \hat{b}]$ and $[\hat{a}, \hat{b}]_+$ are commutator and anti-commutator of two operators \hat{a} and \hat{b} , respectively. The EOM (6) requires the knowledge of the 2-RDM. Similarly the EOM for the 2-RDM involves the 3-RDM and so on. The resulting system of coupled equations is known as the BBGKY hierarchy (Bogoliubov, Born, Green, Kirkwood, Yvon) [28–33] and is more complicated to solve than the TDSE. Thus any application in practice aims at truncating the hierarchy at some level $q < N$. As in our case $N = 2$ and we do not want to propagate the 2-RDM (which is of twice the number of dimensions

of the 2-electron wavefunction) we cut the BBGKY hierarchy already after the first equation (6). However, $\hat{\gamma}_1(t)$ still has the same dimensionality as the 2-electron wavefunction. We therefore expand $\hat{\gamma}_1(t)$ and $\hat{\gamma}_2(t)$ in a complete, orthonormal basis of single-particle orbitals $\hat{1} = \sum_{n=1}^{\infty} |n(t)\rangle\langle n(t)|$, $\langle m(t)|n(t)\rangle = \delta_{mn}$,

$$\hat{\gamma}_1(t) = \sum_{mn} \rho_{mn}(t) |m(t)\rangle\langle n(t)|, \quad (7)$$

$$\hat{\gamma}_2(t) = \sum_{ijkl} \gamma_{2,ijkl}(t) |i(t)j(t)\rangle\langle k(t)l(t)|, \quad (8)$$

where the shorthand notation for tensor products $|i(t)j(t)\rangle = |i(t)\rangle^{(1)}|j(t)\rangle^{(2)} = |i(t)\rangle^{(1)} \otimes |j(t)\rangle^{(2)}$ is used, and a superscript index indicates the particle to which states refer. Note that these expansion coefficients are connected via

$$\rho_{mn}(t) = \frac{2}{N-1} \sum_j \gamma_{2,mjn_j}(t) \quad (9)$$

and are formally defined as

$$\rho_{mn}(t) = \langle m(t)|\hat{\gamma}_1(t)|n(t)\rangle, \quad (10)$$

$$\gamma_{2,ijkl}(t) = \langle i(t)j(t)|\hat{\gamma}_2(t)|k(t)l(t)\rangle. \quad (11)$$

By inserting the expansions (7) and (8) into (6) the EOM for the time-dependent orbitals is obtained, which turns out to be the same as the EOM for MCTDHF orbitals,

$$\begin{aligned} i|\dot{n}(t)\rangle = & \hat{R}(t) \left[\left(\hat{h}(t) - i\hat{\Gamma}_e \right) |n(t)\rangle \right. \\ & \left. + 2 \sum_{ijkl} \rho_{kn}^{-1}(t) \gamma_{2,ijkl}(t) \langle l(t)|\hat{v}_{ee}|j\rangle |i(t)\rangle \right] \\ & + \sum_j g_{nj}^T(t) |j(t)\rangle, \end{aligned} \quad (12)$$

where $\hat{R}(t) = \hat{1} - \sum_n |n(t)\rangle\langle n(t)|$ and $g_{mn}(t) = \langle m(t)|\hat{g}(t)|n(t)\rangle = i\langle m(t)|\dot{n}(t)\rangle$ with an arbitrary hermitian operator $\hat{g}(t)$. In order to solve (12) the expansion coefficients $\gamma_{2,ijkl}(t)$ are needed. One possibility is to expand the state in the same truncated orthonormal basis as $\hat{\gamma}_1(t)$ and $\hat{\gamma}_2(t)$,

$$|\Phi(t)\rangle = \sum_{j_1 \dots j_N} d_{j_1 \dots j_N}(t) |j_1(t) \dots j_N(t)\rangle, \quad (13)$$

and propagate the $d_{j_1 \dots j_N}(t)$, which are formally defined as

$$d_{j_1 \dots j_N}(t) = \langle j_1(t) \dots j_N(t) | \Phi(t) \rangle. \quad (14)$$

The EOM for the expansion coefficients $d_{j_1 \dots j_N}(t)$ is obtained by inserting (13) into the TDSE (1) and multiplying from the left with $\langle j_1(t) \dots j_N(t) |$. The $\gamma_{2,ijkl}(t)$ is then calculated from

$$\gamma_{2,ijkl}(t) = \binom{N}{n} \sum_{m_3 \dots m_N} d_{ijm_3 \dots m_N}(t) d_{klm_3 \dots m_N}^*(t). \quad (15)$$

1. Natural orbitals

If one uses the exact expression for $\gamma_{2,ijkl}(t)$ any “gauge choice” for the hermitian operator $\hat{g}(t)$ should give the same result. In practice, the simulation may benefit from a gauge choice leading to EOMs with better numerical properties; for instance, small matrix elements $g_{mn}(t)$ might allow for larger time steps. Common gauge conventions are $g_{ij}(t) = 0$ or $g_{ij}(t) = \langle j(t)|\hat{h}(t)|i(t)\rangle$, where $g_{ij}(t) = 0$ usually allows to use slightly larger time steps.

One can use the gauge freedom of choosing $\hat{g}(t)$ to require that the orbitals $|n(t)\rangle$ are eigenfunctions of the 1-RDM, called natural orbitals (NOs), i.e.,

$$\hat{\gamma}_1(t) = \sum_k n_k(t) |k(t)\rangle \langle k(t)| \quad (16)$$

and $\rho_{mn}(t) = \delta_{mn} n_n(t)$, where $n_k(t)$ are the corresponding eigenvalues, called occupation numbers (ONs). This is possible because the matrix elements $\rho_{mn}(t)$ depend on the gauge choice,

$$\begin{aligned} i\dot{\rho}_{mn}(t) = & i\langle m(t)|\dot{\gamma}_1(t)|n(t)\rangle - \sum_k \rho_{kn}(t) g_{mk}(t) \\ & + \sum_k \rho_{mk}(t) g_{kn}(t), \end{aligned} \quad (17)$$

which is obtained by taking the time derivative of (10) and inserting unities $\hat{1} = \sum_k |k(t)\rangle \langle k(t)|$.

For $n \neq m$ if $n_n(t) \neq n_m(t)$, one finds out that for NOs

$$g_{mn}(t) = \frac{i\langle m(t)|\dot{\gamma}_1(t)|n(t)\rangle}{n_n(t) - n_m(t)}. \quad (18)$$

Note that when $n_n(t) = n_m(t)$ all terms $g_{mn}(t)$ are undetermined. In this case eigenvalues are degenerate and any orthogonal pair of eigenstates from the subspace they span can be chosen. For those terms any value generated by some arbitrary hermitian operator $\hat{g}(t)$ can be chosen (we use $g_{mn}(t) = 0$). Also, all diagonal terms $g_{mm}(t)$ are undetermined because the phases of the NOs (as eigenstates of the 1-RDM) are not defined. Here we use the phase convention presented in [7],

$$\begin{aligned} i\langle n|\dot{n}\rangle = & \frac{1}{2}\langle n|\hat{h}(t)|n\rangle + \frac{1}{2}\langle n'|\hat{h}(t)|n'\rangle \\ & + \frac{1}{n_n(t)} \text{Re} \sum_{jpl} \gamma_{2,plnj}(t) \langle nj|\hat{v}_{ee}|pl\rangle, \end{aligned} \quad (19)$$

which ensures that for two-electron systems $\gamma_{2,ijkl}(t)$ is an adiabatic functional of the ONs [5],

$$\begin{aligned} \gamma_{2,ijkl}(t) &= d_{ij}(t) d_{kl}^*(t) \delta_{i,j'} \delta_{k,l'} \\ &= (-1)^{i-k} \sqrt{n_i(t) n_k(t)} \frac{e^{i[\varphi_i - \varphi_k]}}{2} \delta_{i,j'} \delta_{k,l'}, \end{aligned} \quad (20)$$

where the “prime operator” acts on a positive integer k as

$$k' = \begin{cases} k+1 & \text{if } k \text{ odd} \\ k-1 & \text{if } k \text{ even,} \end{cases} \quad k > 0, \quad (21)$$

and $e^{i\varphi_i}$ are phase factors which, if one allows for complex groundstate NOs, can be set to $e^{i\varphi_i} = 1$.

If one chooses to propagate NOs, one can propagate either the set of NOs and the expansion coefficients for the wavefunction $d_{j_1\dots j_N}(t)$ (as in MCTDHF) or the set of NOs and ONs, using the exact expression or an approximation for $\gamma_{2,ijkl}(t)$. For two-electron systems, it turns out that the second choice is numerically more efficient. Moreover, the propagation according to the EOM for the combined quantity

$$|\tilde{k}(t)\rangle = \sqrt{n_k(t)} |k(t)\rangle, \quad (22)$$

called renormalized NOs (RNOs), is more stable. The EOM for the RNOs read [7]

$$\begin{aligned} i\partial_t |\tilde{n}\rangle = & \left(\hat{h}(t) - i\hat{\Gamma}_e \right) |\tilde{n}\rangle + \mathcal{A}_n(t) |\tilde{n}\rangle \\ & + \sum_{k \neq n} \mathcal{B}_{nk}(t) |\tilde{k}\rangle + \sum_k \mathcal{C}_{nk}(t) |\tilde{k}\rangle, \end{aligned} \quad (23)$$

with

$$\begin{aligned} \mathcal{A}_n(t) = & -\frac{1}{n_n(t)} \text{Re} \sum_{jkl} \tilde{\gamma}_{2,njkl}(t) \langle \tilde{k}\tilde{l}|\hat{v}_{ee}|\tilde{n}\tilde{j}\rangle \\ & - \frac{1}{2n_n(t)} \left(\langle \tilde{n}|\hat{h}(t)|\tilde{n}\rangle - \langle \tilde{n}'|\hat{h}(t)|\tilde{n}'\rangle \right) \\ & - 2i \sum_{jl} \tilde{\gamma}_{2,njnl}(t) \langle \tilde{l}|\hat{\Gamma}_e|\tilde{j}\rangle, \end{aligned} \quad (24)$$

$$\mathcal{C}_{nk}(t) = 2 \sum_{jl} \tilde{\gamma}_{2,kjnl}(t) \langle \tilde{l}|\hat{v}_{ee}|\tilde{j}\rangle, \quad (25)$$

$$\begin{aligned} \mathcal{B}_{nk}(t) = & \sum_p \frac{\langle k(t)|\hat{C}_{np}(t)|p(t)\rangle - \langle n(t)|\hat{C}_{kp}(t)|p(t)\rangle^*}{n_n(t) - n_k(t)} \\ & - 4i \frac{n_n(t)}{n_n(t) - n_k(t)} \sum_{jl} \tilde{\gamma}_{2,kjnl}(t) \langle \tilde{l}|\hat{\Gamma}_e|\tilde{j}\rangle \\ & - 2i \frac{1}{n_n(t) - n_k(t)} \langle \tilde{k}|\hat{\Gamma}_e|\tilde{n}\rangle, \quad n_k(t) \neq n_n(t), \end{aligned} \quad (26)$$

and

$$\tilde{\gamma}_{2,ijkl}(t) = \frac{1}{\sqrt{n_i(t) n_j(t) n_k(t) n_l(t)}} \gamma_{2,ijkl}(t). \quad (27)$$

Note that if one chooses a gauge $\hat{g}(t)$ such that the orbitals are NOs or RNOs it is very important to use the EOM (23) with the imaginary potential taken properly into account. For example, we observed in [5] that during Rabi oscillations the NO with the lowest ON among all NOs taken into account in the numerical propagation shows erratic behavior after a while, subsequently spoiling NOs with higher ONs. In [5] we thought this effect is due to the necessary truncation of the number of NOs considered during propagation, due to which the last NO cannot couple correctly to all other NOs. Now

we know that with the proper EOM (23) (and an imaginary potential instead of a multiplicative mask function to absorb outgoing electron flux) no erratic behavior occurs. Alternatively, one could also use infinite-range exterior complex scaling [34] to absorb outgoing electron flux, with the EOM modified accordingly.

B. Model atom

We employ the widely used one-dimensional helium model atom [35–39] for benchmarking. The Hamiltonian reads

$$\hat{H}^{(1,2)}(t) = \hat{h}^{(1)}(t) + \hat{h}^{(2)}(t) + \hat{v}_{ee}^{(1,2)} - i\hat{\Gamma}_e^{(1)} - i\hat{\Gamma}_e^{(2)} \quad (28)$$

where upper indices indicate the action on either electron 1, electron 2, or both. The single-particle Hamiltonian in dipole approximation and velocity gauge (with the purely time-dependent $A^2(t)$ term transformed away) reads

$$\hat{h}(t) = \frac{\hat{p}^2}{2} - \frac{2}{\sqrt{\hat{x}^2 + \varepsilon_{ne}}} + A(t)\hat{p}, \quad (29)$$

and the electron-electron interaction

$$\hat{v}_{ee}^{(1,2)} = \frac{1}{\sqrt{(\hat{x}^{(1)} - \hat{x}^{(2)})^2 + \varepsilon_{ee}}}. \quad (30)$$

For the imaginary potential we chose

$$\hat{\Gamma}_e = 50\hat{\xi}^{16}, \quad \hat{\xi} = \begin{cases} \hat{x}/x_{\max} & \text{if } x > 0 \\ 0 & \text{if } x = 0 \\ \hat{x}/x_{\min} & \text{if } x < 0, \end{cases} \quad (31)$$

where $x_{\min} < 0$ and $x_{\max} > 0$ are the coordinates of the left and right boundaries of the 1D grid, respectively. The values for the parameters $\varepsilon_{ne} = 0.50$ and $\varepsilon_{ee} = 0.33$ were chosen to match the real, three-dimensional He and He^+ ionization potentials.

III. RESULTS

Results from TDRNOT and MCTDHF calculations for SPDI, together with the corresponding TDSE benchmark, will be presented in this Section. All results were obtained starting from the spin-singlet ground state, which was calculated via imaginary-time propagation. Real-time propagation was performed with enabled imaginary potential on an equidistant grid with 1024 grid points (in each spatial direction) with a grid spacing of 0.2. An adaptive time step via the Dormand–Prince RK 5(4) method [40] was used in the MCTDHF and TDRNOT calculations.

A. Single-photon double ionization

SPDI is yet another effect where TDDFT does not work in practice, especially if one is interested in correlated photoelectron spectra, for which no density functional is known.

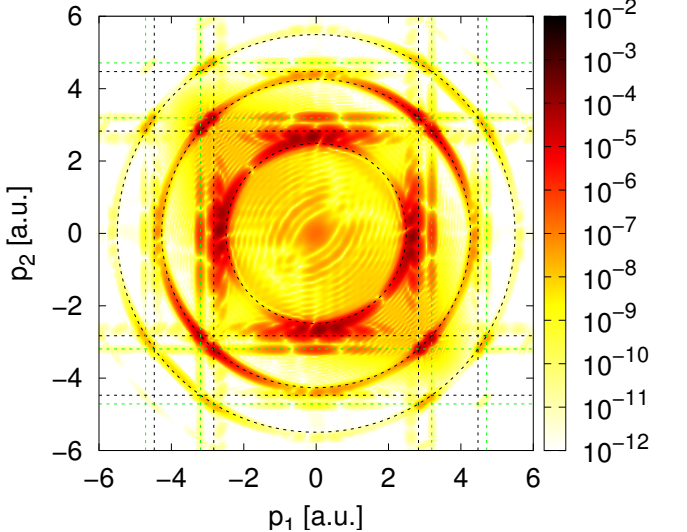


FIG. 1. (Color online) Correlated photoelectron momentum spectrum calculated from the TDSE by applying a filter in position-space [6, 15]. A 7.6-nm 20-cycle \sin^2 -shaped laser pulse of peak intensity $I_0 = 3.2 \times 10^{15} \text{ W/cm}^2$ was used. The dashed green vertical and horizontal lines indicate the photoelectron momenta after single ionization of He by absorbing one, two, and three photons. The dashed black vertical and horizontal lines indicate the photoelectron momenta after ionization of He^+ by absorbing one, two, and three photons.

If $\hbar\omega > |E_0^{\text{He}}|$ one photon can fully ionize a helium atom. However, electron-electron interaction is required in order to share the photon energy absorbed by one electron with another electron. From energy conservation, one obtains

$$E_{\text{kin}}^{(1)} + E_{\text{kin}}^{(2)} = \hbar\omega + E_0^{\text{He}}, \quad (32)$$

where $E_{\text{kin}}^{(i)}$ is the kinetic energy of the i -th photoelectron. As a consequence, one expects a ring of radius $p = \sqrt{2(\hbar\omega + E_0^{\text{He}})}$ in correlated photoelectron momentum spectra. If both electrons are emitted in the same direction it is very improbable that one will measure both electrons with the same kinetic energy due to Coulomb repulsion. It is more likely that one electron will have a higher kinetic energy than the other. Thus, we expect the probability along the SPDI-ring to vary. In fact, this is seen in Fig. 1. There is a minimum on the SPDI-ring if both photoelectrons have the same energy and are emitted in the same direction.

An atom can simultaneously absorb also two and more photons. If n is the number of photons which are simultaneously absorbed then the atom can be fully ionized if $n\hbar\omega > |E_0^{\text{He}}|$. Thus, if the photon energy $\hbar\omega > |E_0^{\text{He}}|$, rings of radius $p = \sqrt{2(n\hbar\omega + E_0^{\text{He}})}$ with $n \in \{1, 2, 3, \dots\}$ are expected in correlated photoelectron momentum spectra. The probability to simultaneous absorb multiple photons decreases exponentially with the number of photons. Three rings can be identified in Fig. 1, and some traces of a fourth one. In order to observe more rings (within a dynamic range of ten orders of magnitude, as in Fig. 1) the laser intensity has to be increased.

The dashed vertical and horizontal lines in Fig. 1 indicate the expected photoelectron momenta after single ionization of He (green) and He^+ (black) by one, two, three photons. An enhanced ionization probability is observed when dashed lines of different color cross the higher-order rings ($n = 2, 3, \dots$), corresponding to sequential double ionization. The probability is smeared out due to electron-electron interaction, especially if the electrons are emitted in the same direction. The correlated photoelectron momentum spectra were calculated by applying a filter in position-space [6, 15] instead of projecting out all bound and singly ionized states. As this is not a rigorous approach to calculate photoelectron spectra, traces of bound and singly excited states are still visible in Fig. 1.

To estimate the minimal number of RNOs or determinants required, one may take the first N_o NOs with the highest ONs in (16), calculated from the exact TDSE wavefunction at the end of the laser pulse, to evaluate the observable of interest. Note that this corresponds to a hypothetical TDRNOT simulation without truncation error [5–8], i.e., with an infinite number of NOs taken into account for propagation, but only the dominating N_o NOs used to calculate observables. Comparing Figs. 1 and 2 we find that 38 RNOs are required to accurately reproduce the SPDI-ring $n = 1$. $N_o \gg 1$ indicates that SPDI is a very correlated process, and differential, correlated photoelectron momentum spectra are correlation-sensitive observables. It is interesting to investigate how many RNOs for TDRNOT (or determinants in MCTDHF) are necessary to describe SPDI. In actual TDRNOT/MCTDHF calculations there is a truncation error so that it is expected that more NOs/determinants are needed to reproduce the correlated photoelectron spectra with TDRNOT /MCTDHF than in Fig. 2 where the NOs were calculated from the TDSE wavefunction. Such TDRNOT calculations of correlated photoelectron spectra in the context of nonsequential double ionization (NSDI) were pursued in Ref. [6] where twice as many RNOs were found to be necessary for propagation to obtain similar results. TDRNOT/MCTDHF results for SPDI are shown in Fig. 3. Quite surprisingly, 38 RNOs/determinants are sufficient to describe SPDI well. Thus the truncation error does not play a crucial role for SPDI. This is probably because the laser pulses used for SPDI are of higher frequency and much shorter than in NSDI so that erroneously positioned and unphysical doubly excited states in the two-electron continuum [5] due to truncation play a minor part.

B. Computational effort

As already mentioned, any choice of the hermitian operator $\hat{g}(t)$ will lead to the same results (for a given number of RNOs/determinant) if one technically manages to solve the corresponding EOM. In practice, the simulations benefit from a gauge choice leading to EOM with good numerical properties. For instance, small matrix elements $g_{mn}(t)$ usually allow for larger time steps. Thus, by setting $g_{mn}(t) = 0$, slightly larger average time-steps can be used in MCTDHF than in TDRNOT, as visible from Table I. However, comparing run

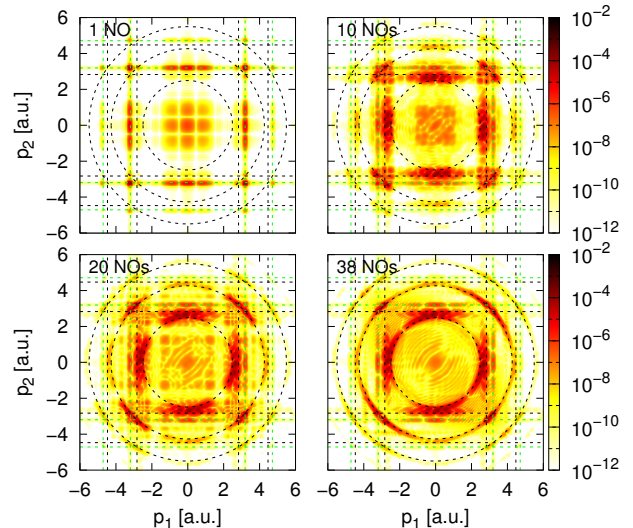


FIG. 2. (Color online) Correlated photoelectron momentum spectra obtained from the first i NOs for $i = 1, 10, 20, 38$, calculated from the TDSE wavefunction at the end of pulse. Same laser pulse as in Fig. 1, dashed lines having same meaning.

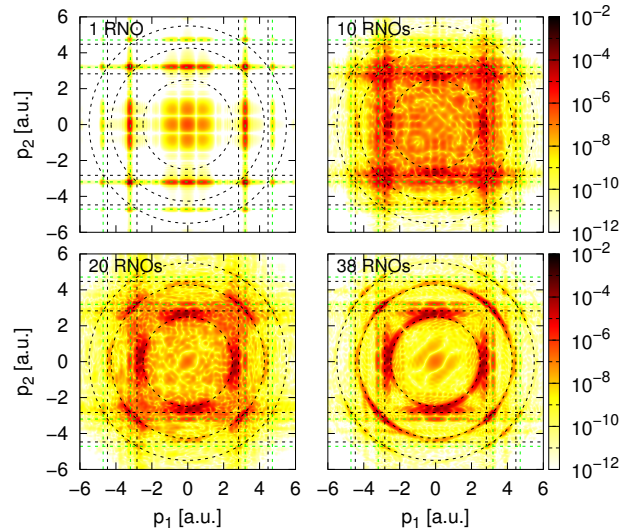


FIG. 3. (Color online) Correlated photoelectron momentum spectrum obtained by TDRNOT/MCTDHF with one to 38 RNOs/determinants. Both methods yield exactly the same spectra when the same number of RNOs/determinants is used. Same laser pulse as in Fig. 1, dashed lines having same meaning.

times one finds that TDRNOT is nevertheless much faster. This is because the analytically known expansion coefficients $\gamma_{2,ijkl}(t)$ for a two-electron system form a sparse matrix in the NO basis but a dense one in MCTDHF. Hence, much less matrix elements need to be calculated in TDRNOT where for 2-electron systems the numerically costly parts of the computations are found to scale as $\tau_{\text{TDRNOT}} \sim N_o^2 N_t N_x \log(N_x)$ vs $\tau_{\text{MCTDHF}} \sim N_o^4 N_t N_x$. Here, N_x denotes the number of grid points and N_t the number of time steps (different gauges lead to different Δt in adaptive propagation schemes). Note

TABLE I. Time (in seconds) required to calculate correlated photoelectron spectra for SPDI with TDRNOT, MCTDHF, and TDSE. The calculations were performed on 4 cores of an i5-3570 processor using $N_x = 1024$ grid points in each spatial direction.

		TDRNOT	MCTDHF	TDSE	MCTDHF/TDRNOT	TDRNOT/TDSE
1 RNO	total time	0.82	1.29	46.99	1.6	0.02
	average Δt	0.0094	0.0093	0.05	1.0	0.19
10 RNO	total time	9.32	247.06	46.99	26.5	0.20
	average Δt	0.0079	0.0102	0.05	1.3	0.16
20 RNO	total time	51.80	6251.75	46.99	120.7	1.10
	average Δt	0.0053	0.0080	0.05	1.5	0.11
38 RNO	total time	467.69	190588.00	46.99	407.5	9.95
	average Δt	0.0031	0.0058	0.05	1.9	0.06

that in Refs. [6, 7] we reported that τ_{TDRNOT} contains also a term $\sim N_\phi^3$. However, by reusing previously calculated quantities it is actually possible to compute everything $\sim N_\phi^2$.

The TDRNOT calculation with 38 RNOs is about 10 times slower than the TDSE. Hence, for the 1D model helium atom TDRNOT does not offer any computational gain. However, as $\tau_{\text{TDSE}} \sim N_t N_x^2$ TDRNOT becomes superior with increasing N_x . Similarly, TDRNOT should be superior for simulations of He in full dimensionality. Unfortunately, it is still unclear if there is any computational gain in TDRNOT over MCTDHF for more than two-electrons. A crucial point here is whether available functionals for $\gamma_{2,ijkl}(t)$ such as PNOF5e [41] and PNOF6(N_c) [42], which are exact in the 2-electron limit, perform well in practice for $N > 2$.

IV. CONCLUSION

In this work, we tested further the recently introduced time-dependent renormalized-natural-orbital theory (TDRNOT) on

singe-photon double ionization (SPDI) of a numerically exactly solvable model helium atom. We showed how TDRNOT is related to multi-configurational time-dependent Hartree-Fock (MCTDHF). We also compared the performance of MCTDHF and TDRNOT, showing that TDRNOT is much faster. Unfortunately, the huge speedup over MCTDHF holds only for two-electron systems. The question whether there is any gain of using TDRNOT over MCTDHF for more-electron systems still needs to be answered and is subject of future work.

ACKNOWLEDGMENT

This work was supported by the SFB 652 of the German Science Foundation (DFG).

[1] F. W. Byron and Charles J. Joachain, “Multiple ionization processes in helium,” *Phys. Rev.* **164**, 1–9 (1967).

[2] Morten Førre, “One-photon double ionization of helium: A heuristic formula for the cross section,” *Phys. Rev. A* **85**, 013420 (2012).

[3] C. Lemell, S. Neppl, G. Wachter, K. Tókési, R. Ernstorfer, P. Feulner, R. Kienberger, and J. Burgdörfer, “Real-time observation of collective excitations in photoemission,” *Phys. Rev. B* **91**, 241101 (2015).

[4] M. Brics and D. Bauer, “Time-dependent renormalized natural orbital theory applied to the two-electron spin-singlet case: Ground state, linear response, and autoionization,” *Phys. Rev. A* **88**, 052514 (2013).

[5] J. Rapp, M. Brics, and D. Bauer, “Equations of motion for natural orbitals of strongly driven two-electron systems,” *Phys. Rev. A* **90**, 012518 (2014).

[6] M. Brics, J. Rapp, and D. Bauer, “Nonsequential double ionization with time-dependent renormalized-natural-orbital theory,” *Phys. Rev. A* **90**, 053418 (2014).

[7] M. Brics, J. Rapp, and D. Bauer, “Strong-field absorption and emission of radiation in two-electron systems calculated with time-dependent natural orbitals,” *Phys. Rev. A* **93**, 013404 (2016).

[8] A. Hanusch, J. Rapp, M. Brics, and D. Bauer, “Time-dependent renormalized-natural-orbital theory applied to laser-driven H_2^+ ,” *Phys. Rev. A* **93**, 043414 (2016).

[9] Jürgen Zanghellini, Markus Kitzler, Thomas Brabec, and Armin Scrinzi, “Testing the multi-configuration time-dependent hartree-fock method,” *J. Phys. B* **37**, 763 (2004).

[10] J. Caillat, J. Zanghellini, M. Kitzler, O. Koch, W. Kreuzer, and A. Scrinzi, “Correlated multielectron systems in strong laser fields: A multiconfiguration time-dependent hartree-fock approach,” *Phys. Rev. A* **71**, 012712 (2005).

[11] David Hochstuhl, Sebastian Bauch, and Michael Bonitz, “Multiconfigurational time-dependent Hartree-Fock calculations for photoionization of one-dimensional Helium,” *J. Phys. Conf. Ser.* **220**, 012019 (2010).

[12] Alejandro Zielinski, Vinay Pramod Majety, and Armin Scrinzi, “Double photoelectron momentum spectra of helium at infrared wavelength,” *Phys. Rev. A* **93**, 023406 (2016).

[13] Carsten A. Ullrich, *Time-Dependent Density-Functional Theory: Concepts and Applications* (Oxford University Press, Ox-

ford, 2011).

[14] Carsten A. Ullrich and Zeng-Hui Yang, “A brief compendium of time-dependent density functional theory,” *Braz. J. Phys.* **44**, 154–188 (2013), arXiv:1305.1388.

[15] F. Wilken and D. Bauer, “Momentum distributions in time-dependent density-functional theory: Product-phase approximation for nonsequential double ionization in strong laser fields,” *Phys. Rev. A* **76**, 023409 (2007).

[16] M. Ruggenthaler and D. Bauer, “Rabi Oscillations and Few-Level Approximations in Time-Dependent Density Functional Theory,” *Phys. Rev. Lett.* **102**, 233001 (2009).

[17] F. Wilken and D. Bauer, “Adiabatic Approximation of the Correlation Function in the Density-Functional Treatment of Ionization Processes,” *Phys. Rev. Lett.* **97**, 203001 (2006).

[18] A.J. Coleman and V.I. Yukalov, *Reduced Density Matrices: Coulson’s Challenge*, Lecture Notes in Chemistry (Springer Berlin Hptageselberg, Berlin, 2000).

[19] Heiko Appel, *Time-Dependent Quantum Many-Body Systems: Linear Response, Electronic Transport, and Reduced Density Matrices*, Ph.D. thesis, Freie Universität Berlin, Berlin (2007).

[20] K. J. H. Giesbertz, *Time-Dependent One-Body Reduced Density Matrix Functional Theory*, Ph.D. thesis, Free University Amsterdam, Amsterdam (2010).

[21] Fabian Lackner, Iva Březinová, Takeshi Sato, Kenichi L. Ishikawa, and Joachim Burgdörfer, “Propagating two-particle reduced density matrices without wave functions,” *Phys. Rev. A* **91**, 023412 (2015).

[22] F. Lackner, I. Březinová, T. Sato, K. L. Ishikawa, and J. Burgdörfer, “Accurate high-harmonic spectra from time-dependent two-particle reduced density matrix theory,” ArXiv e-prints (2016), arXiv:1611.00888 [physics.atom-ph].

[23] Kenichi Ishikawa and Takeshi Sato, “A review on ab initio approaches for multielectron dynamics,” *IEEE J. Sel. Topics Quantum Electron.* **21**, 1–1 (2015).

[24] D. Hochstuhl, C.M. Hinz, and M. Bonitz, “Time-dependent multiconfiguration methods for the numerical simulation of photoionization processes of many-electron atoms,” *Eur. Phys. J. Spec. Top.* **223**, 177–336 (2014).

[25] Loren Greenman, Phay J. Ho, Stefan Pabst, Eugene Kamarchik, David A. Mazzotti, and Robin Santra, “Implementation of the time-dependent configuration-interaction singles method for atomic strong-field processes,” *Phys. Rev. A* **82**, 023406 (2010).

[26] Stefan Pabst and Robin Santra, “Strong-field many-body physics and the giant enhancement in the high-harmonic spectrum of xenon,” *Phys. Rev. Lett.* **111**, 233005 (2013).

[27] Antonia Karamatskou, Stefan Pabst, Yi-Jen Chen, and Robin Santra, “Calculation of photoelectron spectra within the time-dependent configuration-interaction singles scheme,” *Phys. Rev. A* **89**, 033415 (2014).

[28] N. N. Bogoliubov, “Kinetic equations,” *J. Phys. USSR* **10**, 265–274 (1946).

[29] N. N. Bogoliubov and K. P. Gurov, “Kinetic equations in quantum mechanics,” *J. Exp. Theor. Phys. (in Russian)* **17**, 614–628 (1947).

[30] J. Yvon, *La Théorie Statistique des Fluides et l’Équation d’Etat, Actualités Scientifiques et Industrielles*, Vol. 203 (Hermann, Paris, 1935).

[31] John G. Kirkwood, “The statistical mechanical theory of transport processes i. general theory,” *J. Chem. Phys.* **14**, 180–201 (1946).

[32] John G. Kirkwood, “The statistical mechanical theory of transport processes ii. transport in gases,” *J. Chem. Phys.* **15**, 72–76 (1947).

[33] M. Born and H. S. Green, “A general kinetic theory of liquids. i. the molecular distribution functions,” *Proceedings of the Royal Society of London A: Mathematical, Physical and Engineering Sciences* **188**, 10–18 (1946).

[34] Armin Scrinzi, “Infinite-range exterior complex scaling as a perfect absorber in time-dependent problems,” *Phys. Rev. A* **81**, 053845 (2010).

[35] R. Grobe and J. H. Eberly, “Photoelectron spectra for a two-electron system in a strong laser field,” *Phys. Rev. Lett.* **68**, 2905–2908 (1992).

[36] S. L. Haan, R. Grobe, and J. H. Eberly, “Numerical study of autoionizing states in completely correlated two-electron systems,” *Phys. Rev. A* **50**, 378–391 (1994).

[37] D. Bauer, “Two-dimensional, two-electron model atom in a laser pulse: Exact treatment, single-active-electron analysis, time-dependent density-functional theory, classical calculations, and nonsequential ionization,” *Phys. Rev. A* **56**, 3028–3039 (1997).

[38] Demetris G. Lappas and Robert van Leeuwen, “Electron correlation effects in the double ionization of He,” *J. Phys. B* **31**, L249 (1998).

[39] Manfred Lein and Stephan Kümmel, “Exact time-dependent exchange-correlation potentials for strong-field electron dynamics,” *Phys. Rev. Lett.* **94**, 143003 (2005).

[40] J.R. Dormand and P.J. Prince, “A family of embedded Runge-Kutta formulae,” *J. Comput. Appl. Math.* **6**, 19–26 (1980).

[41] M. Piris, J. M. Matxain, and X. Lopez, “The intrapair electron correlation in natural orbital functional theory,” *J. Chem. Phys.* **139**, 234109 (2013).

[42] Xabier Lopez, Mario Piris, Fernando Ruipérez, and Jesus M. Ugalde, “Performance of PNOF6 for hydrogen abstraction reactions,” *J. Phys. Chem. A* **119**, 6981–6988 (2015).